JOURNAL OF GEOPHYSICAL RESEARCH, VOL. 99, NO. D9, PAGES 18,879–18,894, SEPTEMBER 20, 1994

Effects of a polar stratospheric cloud parameterization on ozone depletion due to stratospheric aircraft in a two-dimensional model

David B. Considine
Applied Research Corporation, Landover, Maryland

Anne R. Douglass and Charles H. Jackman
NASA Goddard Space Flight Center, Greenbelt, Maryland

Abstract. A parameterization of Type 1 and 2 polar stratospheric cloud (PSC) formation is presented which is appropriate for use in two-dimensional (2-D) photochemical models of the stratosphere. The calculation of PSC frequency of occurrence and surface area density uses climatological temperature probability distributions obtained from National Meteorological Center data to avoid using zonal mean temperatures, which are not good predictors of PSC behavior. The parameterization does not attempt to model the microphysics of PSCs. The parameterization predicts changes in PSC formation and heterogeneous processing due to perturbations of stratospheric trace constituents. It is therefore useful in assessing the potential effects of a fleet of stratospheric aircraft (high speed civil transports, or HSCTs) on stratospheric composition. The model calculated frequency of PSC occurrence agrees well with a climatology based on stratospheric aerosol measurement (SAM) II observations. PSCs are predicted to occur in the tropics. Their vertical range is narrow, however, and their impact on model O_3 fields is small. When PSC and sulfate aerosol heterogeneous processes are included in the model calculations, the O_3 change for 1980 - 1990 is in substantially better agreement with the total ozone mapping spectrometer (TOMS) -derived O_3 trend than otherwise. However, significant discrepancies in the northern midlatitudes remain. The overall changes in model O_3 response to standard HSCT perturbation scenarios produced by the parameterization are small and tend to decrease the model sensitivity to the HSCT perturbation. However, in the southern hemisphere spring a significant increase in O_3 sensitivity to HSCT perturbations is found. At this location and time, increased PSC formation leads to increased levels of active chlorine, which produce the O_3 decreases.

Introduction

The effects of a fleet of stratospheric aircraft (high speed civil transports, or HSCTs) on the chemistry of the stratosphere have been a subject of considerable interest since the early 1970s [*Johnston,* 1971]. Such a fleet would release significant amounts of NO_x ($NO_x = NO + NO_2$), H_2O, and other compounds directly into the stratosphere. The effluents of the fleet could have a large impact on stratospheric trace constituents and may result in an unacceptable decrease in stratospheric O_3 levels [*Johnston et al.,* 1989].

Various two-dimensional (2-D) photochemical models have been used to gauge the magnitude of the problem [*Ko,* 1992; *Ko and Weisenstein,* 1993; *Ko and Douglass,* 1993]. A 2-D model is a zonally-averaged representation of stratospheric photochemistry and transport. Such models are central to the current assessments of the effects of HSCTs on the stratosphere. They promise to remain so for some time because unlike three-dimensional (3-D) models, their computational requirements are modest enough to allow simulations on a decadal timescale.

Heterogeneous chemical reactions occurring on the surfaces of stratospheric particulates play a very important role in lower stratospheric chemistry. In the polar regions, heterogeneous reactions on polar stratospheric clouds (PSCs) result in the annual formation of the ozone hole during the southern hemisphere spring [*Solomon,* 1990]. Throughout the lower stratosphere, heterogeneous reactions occurring on the stratospheric sulfate aerosol (SSA) layer are important to the partitioning of total odd nitrogen species, which increases

Paper number 94JD01026.
0148-0227/94/94JD-01026$05.00

the sensitivity of O_3 to changes in stratospheric chlorine loading [*Hofmann and Solomon,* 1989; *Considine et al.,* 1992; *Granier and Brasseur,* 1992]. Heterogeneous reactions on SSAs also change model predictions of O_3 depletion due to HSCTs significantly [*Ko and Weisenstein,* 1993]. Models incorporating these reactions predict HSCT-induced column O_3 depletions that are typically 3 to 4 times smaller than those predicted by purely gas phase models. At some locations and times of year, simulations with SSAs included show column O_3 increases with the addition of the HSCT fleet [*Weisenstein et al.,* 1991]. Note that in these studies, the effects of PSCs have not been considered.

SSAs are primarily liquid droplets of H_2SO_4 and H_2O. Conditions are favorable for their formation and growth throughout the lower stratosphere, resulting in a relatively uniform global distribution [*Hamill et al.,* 1977; *Turco et al.,* 1982]. PSCs are divided into two types, denoted Type 1 and Type 2 PSCs. Type 1 PSCs are thought to be primarily frozen nitric acid trihydrate (NAT), while the Type 2 PSCs are frozen H_2O [*Turco et al.,* 1989]. The formation temperatures of these particles are low so they occur most frequently in the polar regions, unlike SSAs.

Because PSCs are largely confined to the poles, it has been thought that their inclusion would only have a small effect on HSCT-induced O_3 depletion. However, stratospheric concentrations of odd nitrogen (NO_y, where $NO_y = N + NO + NO_2 + NO_3 + 2N_2O_5 + HNO_3 + HO_2NO_2 + ClONO_2$) and H_2O are expected to increase significantly from an HSCT fleet [*Douglass et al.,* 1992]. Since the formation of PSCs depends on ambient concentrations of NO_y and H_2O, there is a possibility that the introduction of a stratospheric aircraft fleet would significantly increase the frequency of occurrence of PSCs away from the poles. *Peter et al.* [1991] concluded that an HSCT fleet could double the Type 1 PSC formation probability in the lower stratosphere, at 70° between December and March, with even larger increases for Type 2 PSCs. Clearly, the effects of increases in PSC formation frequencies on predictions of HSCT-induced O_3 depletion should be evaluated.

Prediction of PSC formation in a 2-D model is difficult because 2-D models rely on zonal mean temperature distributions. These are generally too warm to support PSC formation In this paper we discuss a method of calculating Type 1 and Type 2 PSC distributions that uses model HNO_3 and H_2O fields combined with climatological distributions of temperature probability of occurrence obtained from National Meteorological Center (NMC) temperature data. The use of the temperature distributions allows for a more accurate PSC occurrence prediction. The modeled PSCs also respond to HSCT perturbations so that aircraft perturbation scenarios can be conducted. The technique allows the calculation of the probability of cloud occurrence, the amount of HNO_3 and H_2O removed from gas phase in the production of the clouds, and the surface area density of the clouds.

It is important to stress that this parameterization is not a microphysical model of PSCs. It is an attempt to realistically characterize PSC behavior in a 2-D model so that the model can be used for assessments.

The parameterization is first presented and validated by comparison to stratospheric aerosol measurement (SAM) II observations of PSC occurrence. Next, the changes it induces in the model O_3 field are examined. Following this we discuss the effects the parameterization has on the model response to a change in stratospheric chlorine loading and on predictions of O_3 depletion due to an HSCT perturbation.

Model Description

The model used for this study is the Goddard Space Flight Center 2-D stratospheric photochemistry model [*Douglass et al.,* 1989; *Jackman et al.,* 1990]. It has a 10° latitudinal resolution, extending from -85° to +85°, and 30 levels equally spaced in log pressure, from the ground to 0.23 mbar ($\approx$ 60 km in approximately 2-km increments). The model time step is 1 day. A residual circulation is calculated using a 4-year zonal average of NMC temperatures. Heating rates are taken from *Dopplick* [1974] and *Dopplick* [1979] from the ground to 100 mbar, and from *Rosenfield et al.* [1987] from 100 mbar to the top of the model. To increase model speed, family chemistry approximations are used. The model calculates daytime average values of 57 species. Of these, 26 are transported, including H_2O. The model constituent distributions compare favorably with those obtained from other 2-D models [*Jackman et al.,* 1989].

In all runs discussed in this paper a parameterization of heterogeneous reactions on SSAs is included. At each grid point in the model, a background aerosol surface area density is specified. Values of the surface area density are based on an analysis of stratospheric aerosol and gas experiment (SAGE) II satellite data as in chapter 8 of *World Meteorological Organization WMO* [1992]. The surface area densities used represent background conditions during periods of low volcanic activity.

Four heterogeneous reactions are catalyzed by the SSA (and also the PSCs when they are introduced into the model):

$$ClONO_2 + H_2O \rightarrow HNO_3 + HOCl \quad (1)$$
$$ClONO_2 + HCl \rightarrow HNO_3 + Cl_2 \quad (2)$$
$$N_2O_5 + HCl \rightarrow HNO_3 + ClONO \quad (3)$$
$$N_2O_5 + H_2O \rightarrow 2HNO_3. \quad (4)$$

These reactions (occurring on the surfaces of PSC particles) play a critical role in the formation of the Antarctic ozone hole [*Solomon,* 1990, and references therein]. Their rates depend on the surface which catalyzes the reaction. For the SSA, reaction (4) is the most important, and the other reactions are minor contributors. For PSCs, reaction (2) has the largest conversion rate. The above reactions are assumed to occur each time a gas phase $ClONO_2$ or N_2O_5 molecule collides with and successfully adsorbs to a sulfate or PSC

Table 1. Values of the "Sticking Coefficients" for Sulfate Aerosol and NAT Aerosol Heterogeneous Reactions

Reaction	γ (Sulfate)	γ (NAT)
$ClONO_2 + H_2O$	$10^{[1.86-0.0747W(T)]}$	0.006
$ClONO_2 + HCl$	$0.1\gamma_{ClONO_2+H_2O}$	0.3
$N_2O_5 + HCl$	0.0	0.003
$N_2O_5 + H_2O$	0.1	0.0006

Here $W(T) = (T(0.6246\ln(p_{H_2O}) - 14.458) + 3565)/(44.777 + 1.3204\ln(p_{H_2O}) - 0.19988T)$ is the weight percent of the sulfate aerosol [*Hanson and Ravishankara*, 1991].

particle. This assumes that the H_2O and HCl are readily available on the particle surface. We also assume that the reaction products desorb from the surface immediately after the reaction.

Given the above picture of the heterogeneous reaction process, each reaction rate will depend on the surface area density of the aerosol, A (the total surface area available on the particles contained in a unit volume of the atmosphere), the mass accommodation or "sticking" coefficient, γ, and the mean velocity of the incident molecule, v, according to the formula:

$$k_j^i = \gamma_j^i v_l \frac{A_i}{4}, \tag{5}$$

where $i = \{\mathrm{SSA}, \mathrm{NAT}, \mathrm{ICE}\}$ refers to the type of aerosol the reaction proceeds on, $j = \{1, \ldots 4\}$ denotes the number of the equation, above, and $l = \{ClONO_2, N_2O_5\}$ indicates the molecule incident on the aerosol particle [*Hofmann and Solomon*, 1989].

The sticking coefficient, γ, can be interpreted as the probability that a collision of $ClONO_2$ or N_2O_5 with an aerosol particle will result in a reaction. The γ values for the above four reactions have been measured in the laboratory for both sulfate and NAT surfaces. The values used here are given in Table 1.

Table 2. Model Constituent Boundary Conditions

Constituent	1980	1990
CFC-11	173.0	275.0
CFC-12	297.0	468.0
CFC-113	15.3	51.0
CFC-114	3.8	7.0
CFC-115	2.1	5.0
CCl_4	95.0	105.0
HCFC-22	54.0	111.0
CH_3CCl_3	105.0	150.0
Halon-1301	0.6	3.2
Halon-1211	0.5	1.8
CH_3Cl	600.0	600.0
CH_3Br	10.0	10.0
N_2O	302	310.0
CH_4	1525.0	1675.0

All values are given in parts per trillion by volume.

Aircraft Perturbation

All the runs considered in this paper are steady state runs, where the model is run with fixed boundary conditions until a repeating annual cycle is obtained. Two aircraft perturbations are considered with two different sets of boundary conditions. The only aircraft effluents considered here are NO_x and H_2O. The aircraft perturbations are taken from Table 1 of *Ko* [1992]. Two different boundary conditions for ground values of chlorofluorocarbons, N_2O, CH_4, and CO_2 are used. The first set of boundary conditions corresponds to 1980 conditions, with background chlorine levels at about 2.5 parts per billion by volume (ppbv). The second set contains a background chlorine level of about 3.5 ppbv and corre-

Table 3. Global Total O_3 for the Various Runs Discussed

Cl_y	EI	PSC	BASE O_3^G	PERT O_3^G	ΔO_3 (DU)	ΔO_3 (%)	Condition
1980	15	No	294.921	294.228	-0.693	-0.235	Standard
1980	15	Yes	288.711	288.115	-0.596	-0.206	Standard
1990	15	No	291.341	291.118	-0.223	-0.077	Standard
1990	15	Yes	282.610	282.377	-0.233	-0.082	Standard
1980	45	No	294.921	290.668	-4.253	-1.442	Standard
1980	45	Yes	288.711	285.134	-3.577	-1.234	Standard
1990	45	No	291.341	288.287	-3.054	-1.048	Standard
1990	45	Yes	282.610	280.063	-2.547	-0.901	Standard
1980	15	No	299.654	297.178	-2.476	-0.826	High NO_x
1980	15	Yes	294.803	292.485	-2.318	-0.780	High NO_x
1980	15	Yes	288.616	288.064	-0.552	-0.191	No supersat
1980	15	Yes	287.533	286.883	-0.649	-0.226	$r_g \times 0.5$
1980	15	Yes	289.834	289.409	-0.425	-0.147	$r_g \times 2.$

Global Total O_3 for the various runs discussed in this paper. Two constituent flux boundary conditions were used, corresponding to 1980 and 1990 conditions; Two emission indices were considered, 15 and 45. If PSCs were included in the model run, the third column entry is "Yes." The "Base" and "Pert" columns give the global total O_3 for a run without and with the HSCT perturbation, respectively. The next two columns of the table give the HSCT-induced change in global total O_3, in Dobson units and percent, respectively. The final column indicates whether any special conditions other than those specified in the text were used.

sponds to 1990 conditions. These are taken from *WMO* [1990] and are shown in Table 2.

The amount of NO_x and H_2O injected by the aircraft is determined by the quantity and spatial distribution of the fleet fuel usage, and an "Emission Index," which specifies the grams of pollutant emitted per kilogram fuel used. In all cases NO_x and H_2O production from a subsonic fleet is assumed to be part of the background atmosphere and is included in the base model runs. The different combinations of the background atmosphere, HSCT perturbation, and inclusion or absence of PSCs are shown in Table 3.

The latitudinal distribution of fuel use for the subsonic fleet peaks in the northern midlatitudes and is injected below 9 km, largely concentrated between 200 and 300 mbar. The subsonic fleet is assumed to use 17×10^{10} kg/year of fuel, emitting 20.7 grams of NO_x and 1230 grams of H_2O per kilogram of fuel used.

The two different supersonic fleet configurations assume that the HSCT fleet flies between 16.8 and 19.8 km, using 7×10^{10} kg/year of fuel. In both cases the fuel use is concentrated in the northern midlatitudes and tapers off to the north and south. The first case assumes a NO_x emission index (EI) of 15 g/kg, while the second case assumes an EI of 45 for NO_x. In both cases the EI for H_2O is 1230 g/kg. Thus the only difference between the two fleet assumptions is that the second has 3 times the NO_x emissions of the first.

Conventional aircraft engines which might be used in the construction of HSCTs have an EI of 40 to 50. By significantly redesigning the engines, it may be possible to reduce this EI by a factor of 10 [*Miake-Lye*, 1992]. The engines used to power the Concorde, which is the only commercial stratospheric aircraft in existence at this time, have an EI for NO_x of 17-20 [*Broderick et al.*, 1975]. Thus the EI = 45 case and the EI = 15 case bracket the values for conventional engine technology.

Temperature Probability Distributions

Zonal mean temperatures cannot be used to predict PSC cloud formation correctly. Temperature varies with longitude above and below the zonal mean value in a particular latitude band, so a substantial fraction of the band could be below the nucleation temperature for Type 1 (T_n^{NAT}) or Type 2 (T_n^{ICE}) PSCs even though the zonal mean temperature is above the nucleation point. This complicates the construction of a 2-D model representation of PSC formation. Zonal mean temperatures can be avoided by using climatological distributions of the temperature probability of occurrence.

The assumption is made that regions of PSCs will condense or evaporate rapidly as air parcels move into and out of low-temperature regions. With this assumption, the fraction of the volume represented by a model gridpoint in which PSCs can form is equivalent to the fraction of the volume characterized by temperatures which are below T_n^{NAT} or T_n^{ICE}. This is equivalent to the fraction of the temperature probability distribution which is below T_n^{NAT} or T_n^{ICE} [*Peter et al.*, 1991].

The temperature distributions were obtained from NMC temperature data for the period from January 1989 to May 1992. For each month, pressure level, and 10° latitude band we counted the number of times each temperature value in the data set occurred. This number, divided by the total number of temperature values reported, gives the probability for finding a particular temperature as a function of latitude, pressure, and month. The resulting function is $P(T, \phi_i, p_j, m_k)$, where $\phi_i = (-85°, -75°, \ldots, +85°)$ are the latitude coordinates, $\{p_j\}$ are the NMC pressure levels, and m_k gives the month.

Two examples of these distributions are shown in Figure 1a and Figure 1b. The solid line in Figure 1a represents the January 50 mbar, 60°-70° distribution. The solid line in Figure 1b describes the January temperature distribution at 100 mbar, 0°-10°. Figure 1b shows that the tropical lower stratosphere is characterized by stable temperatures and a sharply peaked distribution. Figure 1a shows that the northern midlatitude winter lower stratosphere has large temperature variations and

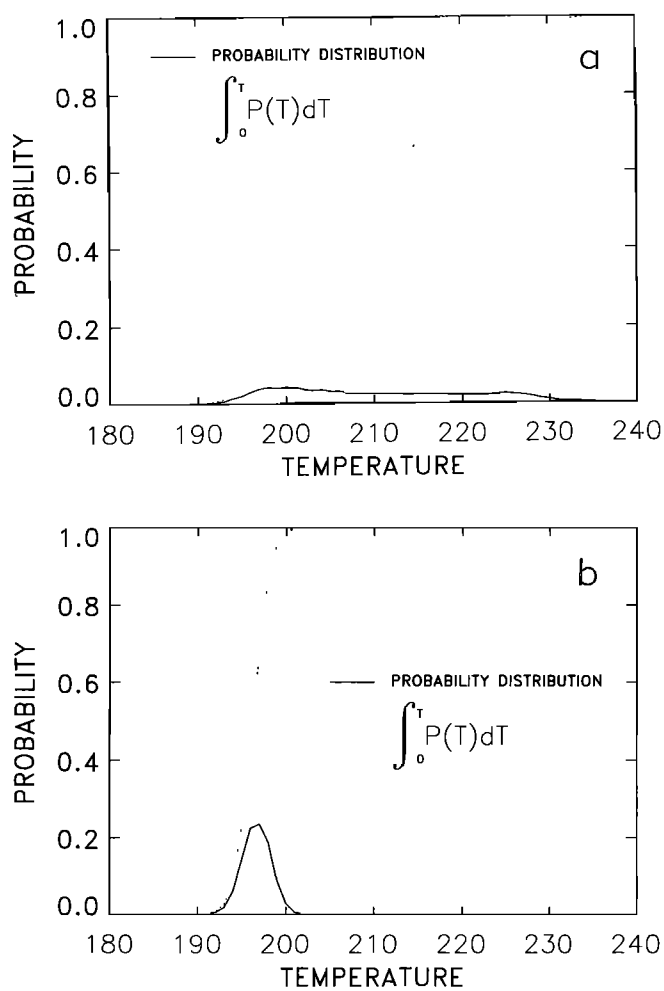

Figure 1. (a) Solid line indicates normalized probability distribution characterizing the January stratosphere at 50 mbar, for the latitude range 60°-70°. Dashed line indicates the fraction of the distribution lying below the temperature T given by the abscissa. (b) Same as Figure 1a,, for the latitude range 0°-10° at 100 mbar.

therefore a broad distribution. In both the high latitude winter and equatorial lower stratosphere, temperatures cold enough to support PSC formation are reached. The dashed lines on each of the two figures give the fraction of the distribution below any particular temperature T. The slope of this line indicates the sensitivity of the regions to changes in PSC formation temperatures. If the slope is steep, then a small increase in the PSC formation temperature may substantially increase the fraction of the atmosphere cold enough to support PSC formation. The sharpness of the tropical temperature distribution shows that for a certain temperature range, the region may be more sensitive to increases in PSC critical temperatures than the mid to high latitudes.

Condensation and Evaporation of Polar Stratospheric Clouds

In order to predict the formation of PSCs, we use equilibrium vapor pressure measurements of H_2O and HNO_3 over NAT as a function of temperature from *Hanson and Mauersberger* [1988]. We also use equilibrium vapor pressure measurements of H_2O over ice from *Marti and Mauersberger* [1993]. These empirical relationionships allow a calculation of the temperature at which a cooling parcel of air with the concentrations $[HNO_3]$ and $[H_2O]$ becomes saturated with respect to NAT or ice (T_s^{NAT} and T_s^{ICE}, respectively). At these temperatures, NAT or ice aerosols may begin to form. Note that dropping below the saturation temperature is a necessary but not sufficient condition for the formation of Type 1 or Type 2 PSCs. There may be other factors needed to induce particle nucleation, such as appropriate condensation nuclei or the need for a supersaturation. Theoretical work and measurements indicate that supersaturation significantly alters the PSC nucleation probability [*Poole et al.*, 1990; *Wofsy et al.*, 1990; *Peter et al.*, 1991; *Dye et al.*, 1992]. *Peter et al.* [1991] have suggested that a supersaturation of the order of 3 K is required to nucleate NAT clouds and 2 K to nucleate ice clouds.

In this study we assume that Type 1 PSCs will nucleate when an ≈3 K supersaturation (supersaturation ratio $s_{NAT} = 10$) is obtained, and Type 2 PSCs will nucleate when an ≈2 K supersaturation exists (supersaturation ratio s_{ICE}=1.4). Evaporation of the aerosols occurs when the parcel temperature rises above the saturation temperatures for the two aerosol types.

Given model distributions of HNO_3 and H_2O, the equilibrium vapor pressure measurements, and the NMC temperature distributions, the fractions of the temperature distribution below T_s^{NAT}, T_s^{ICE}, T_n^{NAT}, and T_n^{ICE} can be calculated as a function of month m, latitude ϕ_i, and pressure p_j. For example, denoting the saturated fraction for NAT aerosols by f_s^{NAT},

$$f_s^{NAT}(T_s^{NAT}, \phi_i, p_j, m_k) = \int_0^{T_s^{NAT}} P(T, \phi_i, p_j, m_k)dT. \quad (6)$$

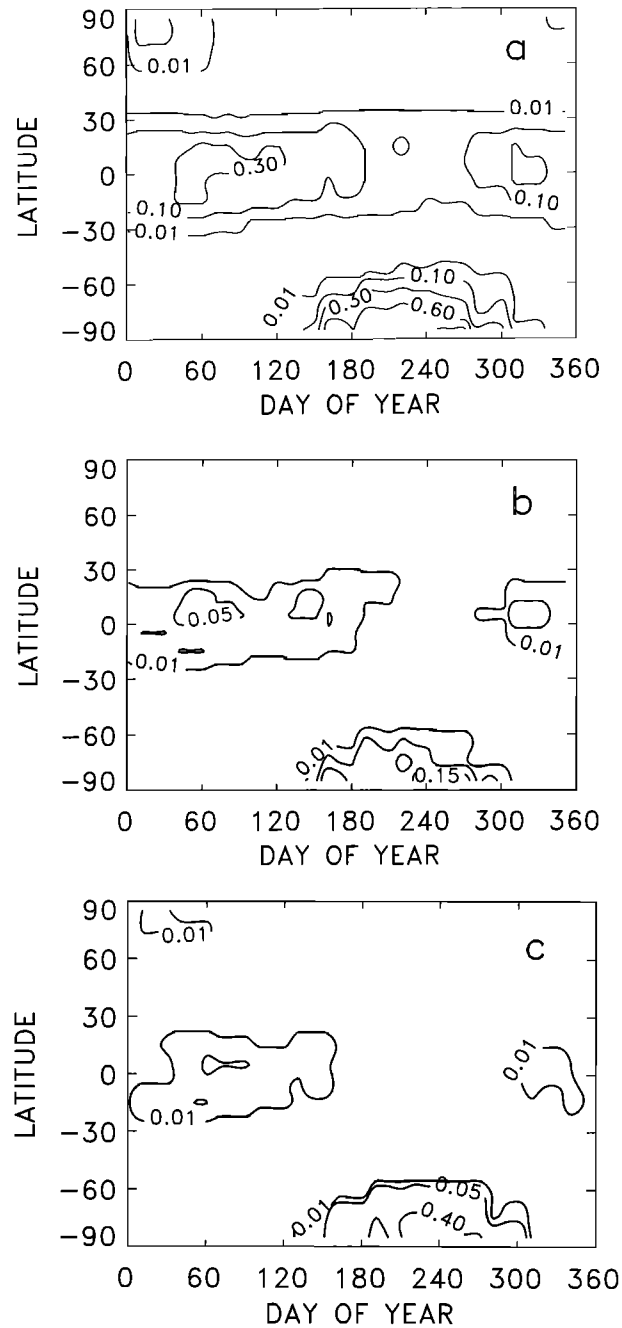

Figure 2. (a) Fraction of atmosphere saturated with respect to NAT aerosols as a function of day and latitude, for the 120-mbar model level. Because $T_s^{NAT} > T_s^{ICE}$, the regions saturated with respect to ice will also be saturated with respect to NAT. Thus $f_s^{NAT} \approx f_s^{PSC}$. (b) Fraction of atmosphere saturated with respect to ice aerosols as a function of day and latitude for the 120-mbar model level. (c) Fraction of atmosphere below NAT nucleation temperature as a function of day and latitude for the 120-mbar model level. A saturation ratio of 10 is assumed.

The quantities f_s^{NAT} and f_s^{ICE} can be thought of as the fractions of the volume represented by a model gridpoint that is saturated with respect to Type 1 and Type 2 PSCs, respectively. Alternatively, they can be considered to be the probabilities that the gridbox is saturated

with respect to the different aerosol types. The nucleation fractions f_n^{NAT} and f_n^{ICE} give the probabilities that nucleation of PSCs occurs in the gridbox at a particular location and time.

A plot of f_s^{NAT} on the 120-mbar surface is shown as a function of latitude and season in Figure 2a. The 120-mbar surface is considered because the values of f_s^{NAT} in the tropics are largest on this pressure surface. Also, the northern and southern hemisphere distributions on the 120-mbar surface are representative of higher altitude distributions. The largest magnitudes are in the southern hemisphere at high latitudes in early September, where up to 0.8 of the region can be saturated with respect to NAT aerosols. Since the regions saturated with respect to ice aerosols are generally also saturated with respect to NATs, f_s^{NAT} is also roughly f_s^{PSC}, the fraction of the region saturated with respect to either type of PSC.

In the northern hemisphere f_s^{NAT} peaks in mid January, where up to 0.15 of the region at high latitudes is saturated with respect to NATs. At some times of the year, the tropics are saturated more frequently with respect to NATs than the northern hemisphere high latitudes. The tropical peak occurs in late February and early March, with peak values over 0.4. However, the vertical extent of the tropical region is much more limited than the regions of significant saturation at high latitudes. At 90 mbar the values in the tropics have dropped off by an order of magnitude, while the polar values remain essentially the same. Polar values begin to drop off appreciably above 30 mbar.

Figure 2b shows the saturated fraction for ice aerosols, f_s^{ICE}, on the 120-mbar surface. In the northern hemisphere the values are below 0.01. The tropical peak reaches above 0.05 in late February, and in the southern hemisphere the peak of 0.15 occurs in September at high latitudes. The vertical extent of the ice-only saturated regions are similar to f_s^{NAT}.

As mentioned above, the probability that PSCs nucleate is not generally equivalent to the probability that the atmosphere becomes saturated with respect to PSC formation. Figure 2c shows the NAT nucleation probability on the 120-mbar surface, which can be compared with Figure 2a. In the northern hemisphere and the tropics, the nucleation probabilities are much smaller than the saturation probabilities at the same location. In the southern hemisphere the nucleation probabilities are substantially smaller than the saturation probability, but the differences between the two quantities are not large compared to the northern hemisphere and tropical differences. The same relationships apply at higher altitudes as well.

The probability that a PSC exists at a particular location is not equivalent to either the saturation or the nucleation probability. Instead, the quantity should be bracketed by the saturation and nucleation probabilities. If a region drops below the nucleation temperature and a PSC forms, the PSC can remain when the region warms above the nucleation temperature, as long as the temperature does not exceed the saturation temperature.

It is interesting to compare the saturation and nucleation probabilities calculated above with satellite observations of PSC frequencies of occurrence. If supersaturation effects do not significantly affect the frequency of PSC occurrence, then the observed PSC frequency of occurrence and the saturation probability should approximate each other. If supersaturation effects strongly influence the frequencies of occurrence, then the observed values should be closer to the nucleation probability. A sighting frequency climatology for PSCs has been constructed for the 1979-1989 period using the SAM II instrument on the Nimbus 7 satellite [*Pitts et al.*, 1991; *M. C. Pitts*, private communication, 1993]. The sighting frequency is the number of observations in which PSCs are observed divided by the total number of observations at a particular altitude, latitude, and time.

Figures 3a and 3b show the SAM II cloud sighting frequency in the northern and southern hemispheres, respectively. Superposed on the observed contours is

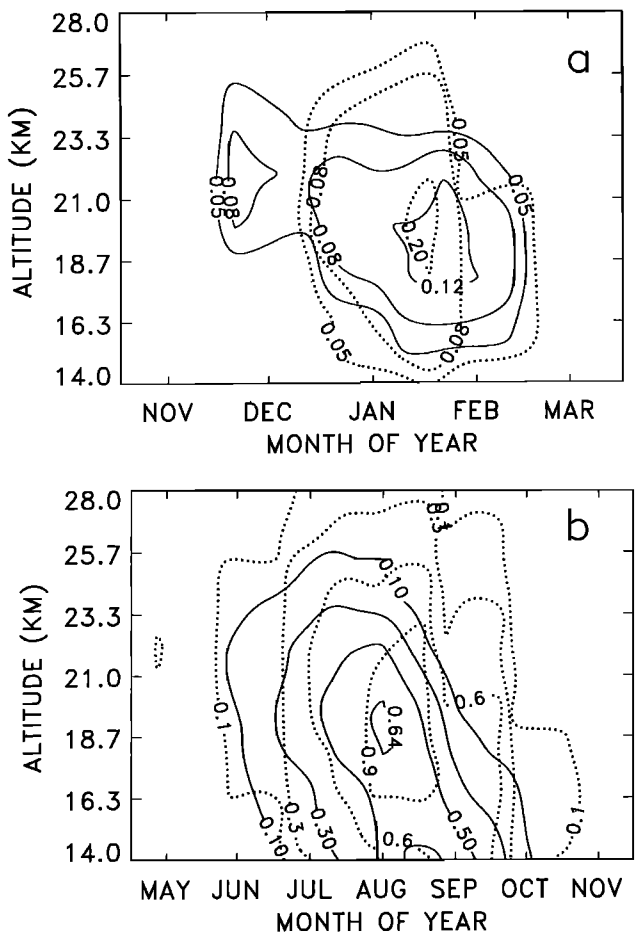

Figure 3. (a) SAM II cloud sighting frequency, northern hemisphere (solid contours) and model calculated fraction of atmosphere saturated with respect to PSCs (dotted contours). Solid lines indicate the fraction of the total number of SAM II observations in which PSCs were observed. (b) SAM II cloud sighting frequency, southern hemisphere (solid contours) and model calculated fraction of atmosphere saturated with respect to PSCs (dotted lines).

the model calculated f_s^{PSC} (dotted lines). The observation latitude of the SAM II measurements varies from 64° at the solstices to 82° at the equinoxes [*McCormick and Trepte*, 1986], and the model calculated values have been interpolated to the same latitudes. There is fairly good agreement between the satellite data and the calculation. The calculated northern hemisphere peak value of just over 0.2 is somewhat higher in magnitude than the observed peak value of 0.14. The peaks are essentially collocated given the 10-day time resolution and 2-km altitude resolution of the data. The observed peak values descend about 2 km over the course of the winter; this descent is not seen in the the calculated values.

The southern hemisphere comparison is shown in Figure 3b. The peak calculated saturated fractions of well over 0.9 are significantly higher than the observed probability of PSC occurrence. The peak calculated values occur in the same location as the observed values, and the onset and disappearance of significant PSC occurrence takes place near the same time as the calculations. As in the northern hemisphere, the maximum observed values descend as the season progresses, but not the calculated values. This may indicate that the calculated sedimentation velocities for the PSCs are too weak.

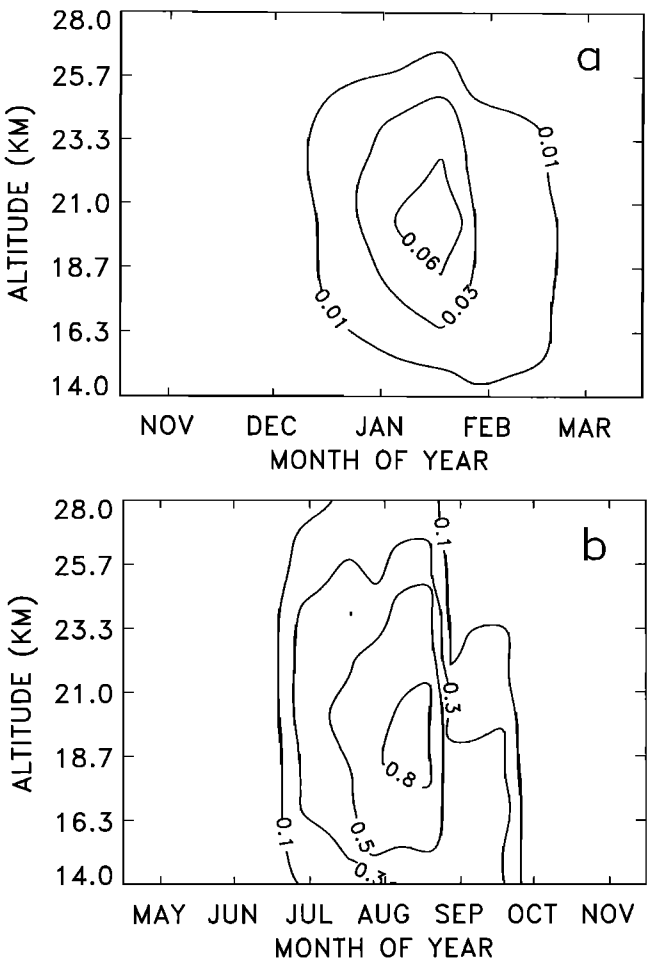

Figure 4. (a) Model calculated fraction of atmosphere where nucleation can occur, northern hemisphere. (b) Model calculated fraction of atmosphere where nucleation can occur, southern hemisphere.

The calculated nucleation probabilities for the northern and southern hemispheres are shown in Figures 4a and 4b, respectively. The nucleation probability is significantly smaller than the saturation probability and the observed frequency of PSC occurrence. In the southern hemisphere the nucleation probability and the saturation probabilities are not as different as the northern hemisphere values are. The peak nucleation probabilities exceed the peak observed PSC occurrence frequencies in the southern hemisphere.

The calculated and observed fields do not match well enough to draw conclusions about the importance of supersaturation effects on PSC frequencies of occurrence. Some of the discrepancy may be due to error in the temperature probability distributions. If this is the case, then it may be possible to obtain better agreement using a longer temperature record in the construction of the distributions. However, the above comparisons of observations and calculation demonstrate that using atmospheric temperature statistics in a 2-D model can reproduce observed PSC occurrence reasonably well.

There is no observational information about tropical NAT cloud occurrence, and thus there is no way to validate the calculation in the tropics. Two-dimensional models tend to underestimate the amount of NO_y present in the equatorial lower stratosphere when compared to limb infrared monitor of the stratosphere (LIMS) measurements [*Ko et al.*, 1986; *Jackman et al.*, 1987]. Therefore f_s^{NAT} and f_n^{NAT} are likely to be underestimated in the tropics.

PSC Surface Area Density Distributions

To assess the effects of PSC formation on predictions of aircraft-induced O_3 depletion, it is necessary to determine the surface area density distribution characterizing the clouds that form. This can be accomplished using temperature probability distributions. Consider a parcel of air that cools to a temperature $T < T_n^{NAT}$. Assume that the parcel has an ambient HNO_3 number density $[HNO_3]$. Condensation in this parcel will begin when $[HNO_3] > s_{NAT}[HNO_3]_{NAT}(T)$, where s_{NAT} is the supersaturation ratio and $[HNO_3]_{NAT}(T)$ is the HNO_3 number density in equilibrium with NAT aerosols at temperature T. The amount of HNO_3 that will condense is simply the difference:

$$\Delta[HNO_3](T) = [HNO_3] - [HNO_3]_{NAT}(T). \quad (7)$$

For this paper we use a supersaturation ratio $s_{NAT} = 10$. This corresponds to an approximately 3 K reduction in the temperature at which NAT aerosols will form and is in accord with calculations [*Peter et al.*, 1991] and observational evidence [*Dye et al.*, 1992; *Kawa et al.*, 1992] for the typical atmospheric supersaturation ratios necessary to nucleate NAT aerosols.

The temperature probability distribution characterizing the atmosphere at a particular latitude, altitude,

and month is given by $P(T, \phi_i, p_j, m_k)$, as described above, and $P(T, \phi_i, p_j, m_k)dT$ gives the fraction of the atmosphere during the month at (ϕ_i, p_j) that exists at the temperature T. This can therefore be used as a weighting function to determine the total amount of HNO_3 that condenses at (ϕ_i, p_j):

$$[HNO_3]_R(\phi_i, p_j) = \int_0^{T_s^{NAT}} \Delta[HNO_3](T)P(T, \phi_i, p_j, m_k)dT. \quad (8)$$

This amount of HNO_3 is subtracted from the gas phase and added to the solid phase burden at that gridpoint. To convert $[HNO_3]_R$ to surface area density, we assume that every condensed-phase HNO_3 molecule is associated with 3 H_2O molecules. Given the molecular weights of the molecules, and assuming the mass density of NAT to be 1.6 g/cm^3 [*Wofsy et al.,* 1990], the total volume of NAT which condenses per cubic centimeter can be calculated. To convert this to surface area density, an assumption about the particle size distribution and characteristic particle size must be made. We assumed a lognormal distribution with a mode radius $r_g = 1$ μm and standard deviation $\sigma = 1.8$.

A similar procedure can be used to determine the amount of H_2O that is removed from gas phase by condensation of Type 2 PSCs. To calculate the surface area density we assumed a lognormal distribution with mode radius $r_g = 10$ μm and standard deviation $\sigma = 1.8$. The supersaturation ratio used was $s_{ICE} = 1.4$, which corresponds approximately to a 2 K reduction in the condensation temperature.

We assume that the aerosols are advected as passive tracers and are also subject to particle sedimentation. The sedimentation velocity used is that of the particle mode radius, calculated according to *Kasten* [1968]. In gridboxes where ice aerosols form, the NAT aerosols sediment at the same velocity as the ice aerosols for that fraction of the gridbox that is saturated with respect to both ice and NAT. This is done with the idea that the NAT aerosols in a region where ice aerosols form act as condensation nuclei for the ice, and are therefore sedimented out at the same velocity as the ice particles. Sedimentation of NAT and ice aerosols produces strong denitrification and dehydration of the southern hemisphere high latitude during late winter and spring. Northern hemisphere high-latitude dehydration and denitrification occurs but is relatively weak.

The surface area density calculated for NAT and ice aerosols on the 120-mbar surface is shown in Figures 5a and 5b. In the northern hemisphere, the NAT surface area density maximizes at high latitudes in January, with peak values around 0.3 μm^2/cm^3. The tropical surface area density peaks in March at approximately 0.09 μm^2/cm^3, and the southern hemisphere peak value of about 2 μm^2/cm^{3}occurs in June. It is interesting to note by comparison with Figure 2a that even though the tropical region is more frequently saturated with respect to NAT than the northern hemisphere high latitudes, the surface area densities at high latitudes exceed the tropical values by over a factor of 3. Tropical temperature variation is significantly smaller than the high-latitude winter; excursions below T_n^{NAT} are more common in the tropics but do not appear to be large enough to condense much NAT.

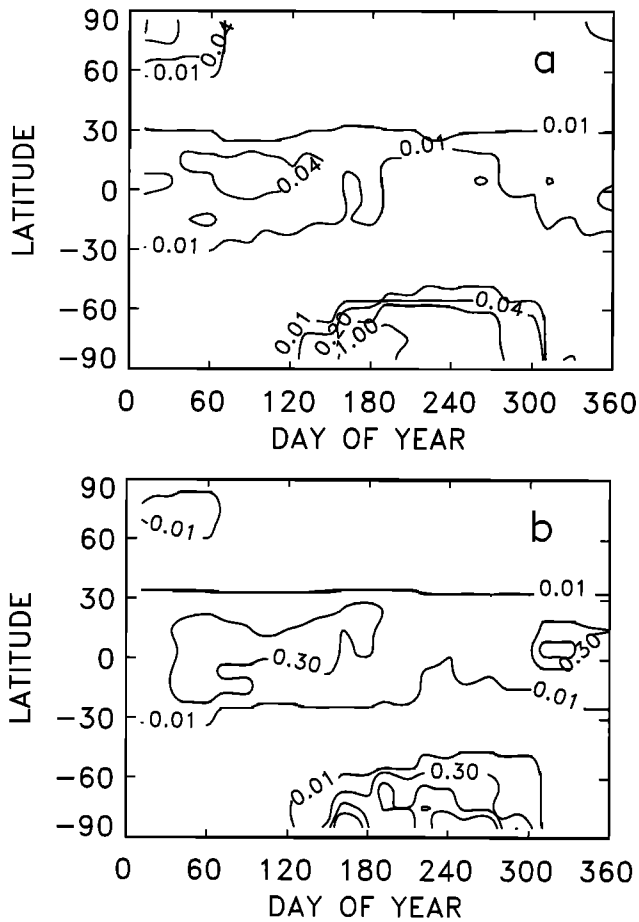

Figure 5. (a) Annual variation of NAT surface area density as a function of latitude on the 120-mbar model surface. Contours: 0.01, 0.04, 0.2, and 1.0 μm^2/cm^3. (b) Annual variation of ice aerosol surface area density as a function of latitude on the 120-mbar model surface. Contours: 0.01, 0.3, 1.0, and 1.5 μm^2/cm^3.

The ice aerosol surface area density in the northern hemisphere is quite small, but in the tropics the values exceed the calculated NAT surface area densities by about a factor of 2. This occurs even though the region is saturated with respect to ice formation (Figure 2b) less frequently than with respect to NATs. In the southern hemisphere, peak surface area densities are about a factor of 3 larger than the peak NAT values.

The vertical extent of the tropical surface area densities is narrow; at the poles the surface area densities for NATs remain high up to 30 mbar in both the northern and southern hemisphere. At the high latitudes, ice surface area densities decrease more rapidly with altitude than the NAT values do, with close to an order of magnitude decline in peak values between 120 and 50 mbar.

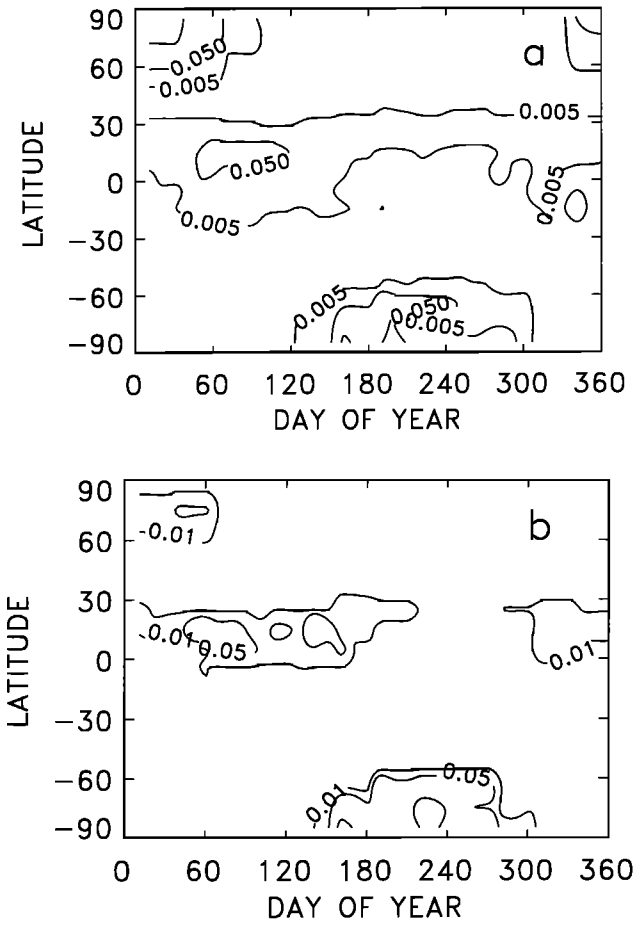

Figure 6. (a) Increase in NAT surface area density as a function of latitude on the 120-mbar model surface from the addition of an HSCT perturbation. The emission index = 15 aircraft scenario described in the text is used. Contours: 0.005, 0.05, and 0.3 $\mu m^2/cm^3$. (b) Increase in ice aerosol surface area density as a function of latitude on the 120-mbar model surface from the addition of the HSCT perturbation. Contours: 0.01, 0.05, and 0.3 $\mu m^2/cm^3$.

When the NO_x and H_2O from a fleet of HSCTs is added to the model, NAT and ice aerosol occurrence is increased, as are PSC surface area densities. Figures 6a and 6b show the 120-mbar increase in NAT and ice aerosol surface area densities with the addition of the EI=15, Mach 2.4 HSCT fleet described above. In the northern hemisphere the peak NAT surface area densities are approximately doubled. The same situation holds for the tropics (Figures 6a and 5a). In the southern hemisphere, the increase is about as large as the northern hemisphere increase but is not as large a fraction of the preexisting NAT surface area densities.

The increase in ice surface area density (Figure 6b) in the northern hemisphere high latitudes is also over a factor of 2, although the values are much smaller than the NAT surface area density increases at the same location. Tropical values increase by about 20%. The largest absolute increases in ice aerosols occur in the southern hemisphere high latitudes.

There are significant uncertainties in the calculation of these surface area densities. Model values of H_2O and HNO_3 are used in the calculation. If these are incorrect, then an incorrect PSC calculation will result. The temperature distributions used may not have been taken from a long enough data set to be an accurate representation of atmospheric temperature statistics. The NMC temperature data itself may not be inaccurate. Finally, assumptions have been made about the size distribution of the aerosols and the supersaturations needed to nucleate them.

The particle size distribution is actually sensitive to the rate at which parcels are cooled [*Wofsy et al.*, 1990]. Large systematic spatial differences in the cooling rate of parcels may change the distribution of PSC surface area density as a function of latitude and altitude. The values of the surface area density also depend on the choice of mean radius. Doubling the radius will halve the surface area density, and reducing it by a factor of 2 will increase the surface area density by a factor of 2.

The qualitative results of this paper are not affected by relatively large changes in these assumptions, as is shown in Table 3. Further, very little is known about the temperature histories of parcels in which PSCs are observed, so there is no way to include cooling rates in the calculation of PSC surface area densities. Finally, the calculated surface area densities are consistent with estimates of particle surface area densities derived from measurements. [*Dye et al.*, 1992]. We conclude that the calculated distributions are sufficiently accurate for assessment purposes.

Effects of PSCs on Ozone

When the PSC parameterization described above is incorporated into the model, the model fields respond to the heterogeneous reactions catalyzed by the clouds, the sequestering of gas phase HNO_3 and H_2O into cloud particles, and to permanent denitrification and dehydration. As a result, column O_3 decreases significantly. The largest reductions occur in the southern hemisphere high latitudes, in late spring and early summer. Figure 7a shows the column O_3 predicted by the model for 1990 boundary conditions, without PSCs. When PSCs are introduced, the column O_3 responds, as seen in Figure 7b. The southern hemisphere high latitudes show a feature similar to the O_3 hole which begins in late August and reaches its maximum depth in early to mid November. The percent reduction in column O_3 caused by the introduction of the PSC parameterization is shown in Figure 7c. The maximum reduction in the southern hemisphere high latitudes is about 45%.

The model southern hemisphere O_3 minimum occurs later in the year than the observed Antarctic O_3 minimum. This is probably due to the model residual circulation and the fact that parcels of air in the 2-D model are not subjected to insolation from nonzonal parcel excursions such as exist in the real atmosphere. The appearance of the O_3 minimum is delayed because photolytic reactions drive the depletion.

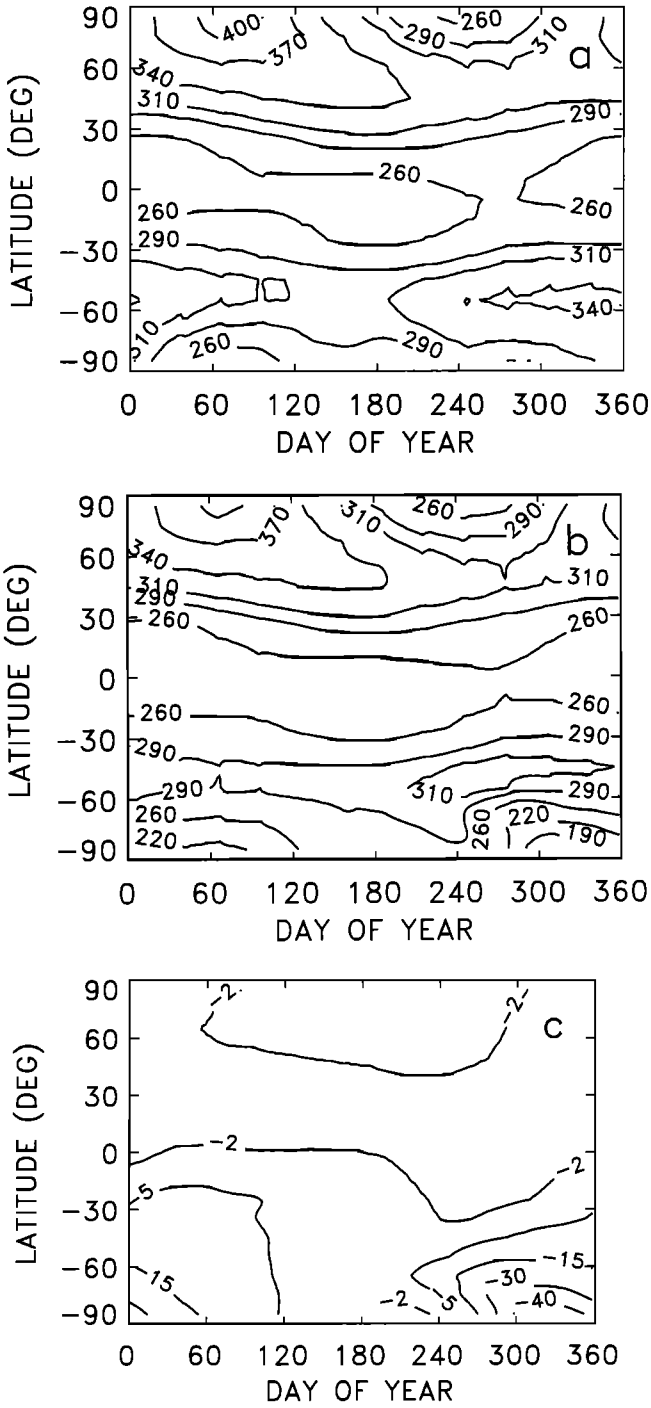

Figure 7. (a) Base case column O_3 calculated for 1990 steady state boundary conditions, without the PSC parameterization (Dobson units). (b) Column O_3 calculated for 1990 boundary conditions, with the PSC parameterization included. An O_3-hole like feature appears in the southern hemisphere high-latitude September- December time period. (c) Percentage change in column O_3 that occurs when the PSC parameterization is added.

The model O_3 "trend" from 1980 to 1990 with the PSC parameterization included can be compared with estimates of the atmospheric trend, which has been calculated using the Nimbus 7 TOMS data [*Stolarski et al.,* 1991]. Figure 8a shows the calculated percentage change of column O_3, in %/year, between the 1980 and 1990 cases. The spatial variation of the trend is similar to those obtained from the satellite observations, shown in Figure 8b. The southern hemisphere maximum trend is somewhat weaker than the observed trends. The mid-latitude trends in both the southern and northern hemisphere, as well as the northern hemisphere high-latitude trends, are substantially lower than the TOMS-derived result.

The discrepancy between the modeled and observed trends may be an indication that heterogeneous processes in the model are too weak. Other factors may also play a role. For instance the smaller calculated trend may partially result from differences between the transport characteristics of the 2-D model and the real atmosphere. The 2-D model does not exhibit a strongly isolated winter polar vortex with meridional constituent gradients as steep as is observed. The effects of increased Cl_y in the model at higher latitudes may therefore be mitigated by a more plentiful supply of NO_y from lower latitudes.

Effects of PSCs on Aircraft Perturbation Predictions

The PSC frequencies of occurrence calculated above compare fairly well with SAM II observations, and the parameterization produces the expected changes in column O_3 when it is added to the model. Both Type 1 and 2 cloud formation is considered, as are supersaturation effects and particle sedimentation. The parameterization thus seems to be a reasonable characterization of PSC behavior. Since it responds to increases in NO_x and H_2O from stratospheric aircraft, it can be used to gauge the magnitude of the effect of PSCs on HSCT-induced O_3 depletion.

Figure 9a shows the change in column O_3 resulting from the EI = 15 HSCT perturbation for 1980 boundary conditions in Dobson units (1 DU = 2.69×10^{-16} molecules cm^{-2}), without PSCs. (Note that sulfate aerosol heterogeneous processes are included in all the runs considered here.) The 1980 boundary conditions are considered here because the background chlorine levels are similar to those that would be encountered in the early 21st century, when the fleet would be flying. The maximum decrease in column O_3 is about 3 DU, occurring in October at the northern and southern hemisphere high latitudes. In the northern hemisphere there is a small region in the late spring where column O_3 increases as a result of the the aircraft perturbation.

Figure 9b shows the aircraft-induced change in column O_3 from a simulation which includes the PSC parameterization. Substantial changes in the southern hemisphere response to the HSCT perturbation can be seen by comparing Figures 9a and 9b. The largest reductions in column O_3 occur in mid November rather than early September. The magnitude of the maximum depletion is approximately doubled. Throughout most of the rest of the hemisphere, however, the depletion is not as intense in the run with the parameterization. In the northern hemisphere, column O_3 depletion with the

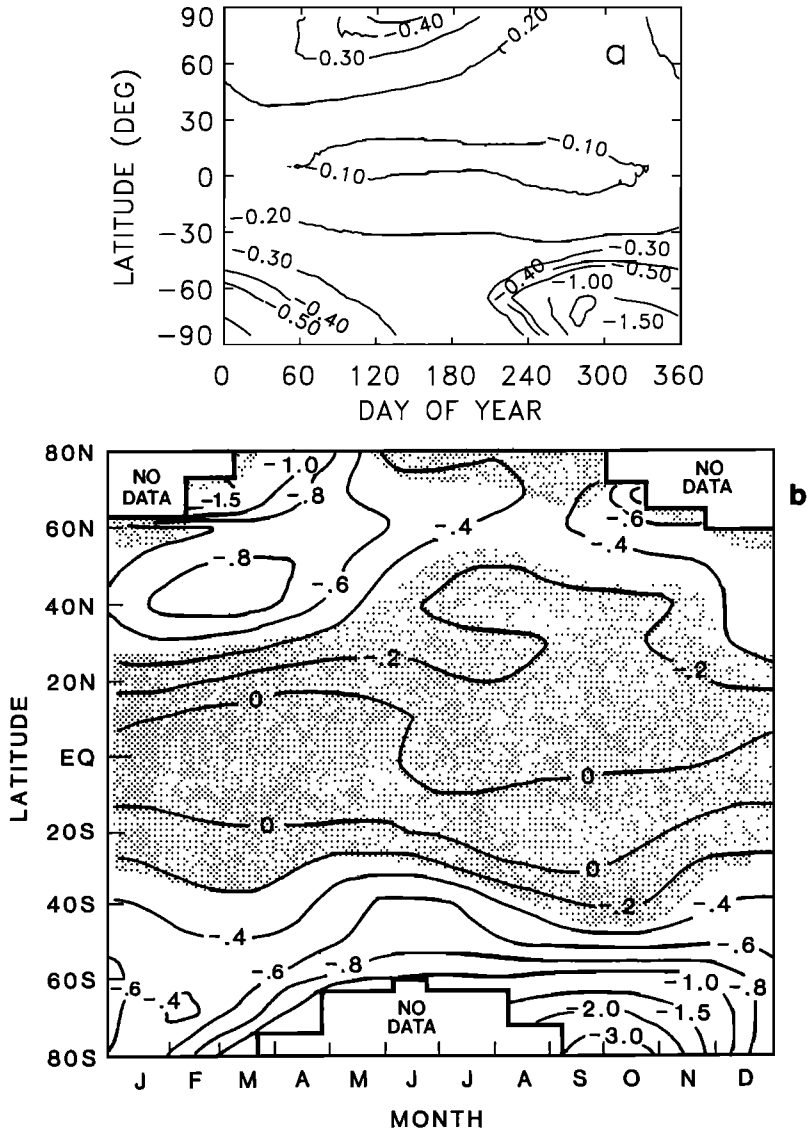

Figure 8. (a) Model calculated O_3 "trend." Figure shows percentage change between two runs with 1980 and 1990 boundary conditions, in %/year. Both runs include PSCs. (b) Observed trend in column O_3 derived from the TOMS instrument on the Nimbus 7 satellite [from *Stolarski et al.*, 1991].

PSC parameterization is not as large as occurs without the parameterization. Also, the column O_3 increases with the PSCs are a bit larger than the increases without the PSCs. The overall effect on global total O_3 is a slight decrease in the O_3 depletion caused by the aircraft. This can be seen in Table 3, which gives the base and perturbed case total O_3 for the runs discussed in this paper.

Figures 9a and 9b show the HSCT-induced changes in terms of Dobson units. It is more conventional to use percent difference, and this is shown in Figures 10a and 10b. In terms of percent difference, the southern hemisphere high latitude O_3 depletion is increased from a 1% depletion to a 3% depletion when PSCs are added to the model calculation. The decrease in the base column O_3 between the no PSC case and the PSC case (Figures 7a and 7b) contributes to this decrease. Using percent differences is somewhat misleading because of the differences in base column O_3 and future comparisons in this paper will be in Dobson units.

Figure 9a shows a southern hemisphere response to the HSCT perturbation that is larger in magnitude than the northern hemisphere response. This is interesting because most of the HSCT emissions are released in the northern hemisphere. Figure 11a shows the increase in NO_x that occurs with the addition of the HSCT fleet to the simulation. The relative maximum seen at about 30°N between 50 and 80 mbar is located at the point of maximum NO_x injection from the fleet. Aside from this region the increase in NO_x from the aircraft is quite symmetric about the equator, and the increases in NO_x at 10 mbar in the high latitudes is similar for both poles.

The symmetry in ΔNO_x results in a fairly symmetric ΔO_3, shown in Figure 11b. At the point of the northern hemisphere relative ΔNO_x maximum is a lower stratospheric increase in O_3. This increase is not observed

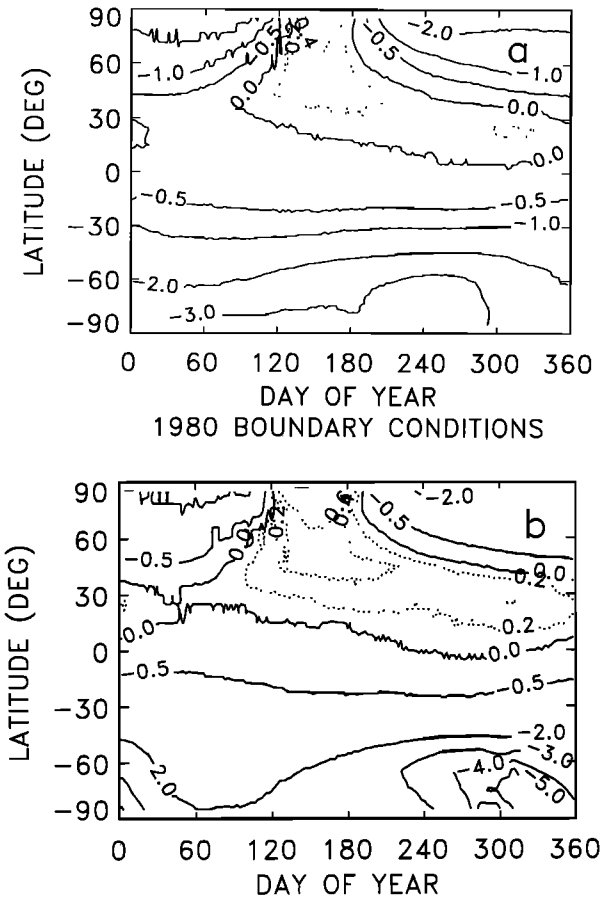

Figure 9. (a) Column O_3 difference between the base case and EI = 15 HSCT perturbation, in Dobson units, without PSC parameterization. Background chlorine levels approximate 1980 conditions. (b) Column O_3 change from the HSCTs with PSCs included.

in the southern hemisphere. The increases here result from an interaction between the CH_4 oxidation process and NO_x, a process which produces O_3 at low altitudes, and interference with HO_x-catalyzed O_3 loss. These lower stratospheric northern hemisphere increases produce the northern hemisphere column O_3 increases seen in Figures 9a and 9b and also result in smaller column O_3 decreases in the northern hemisphere compared to the southern.

Higher levels of model background chlorine reduce the HSCT-induced O_3 depletions and augment the O_3 increases in the northern hemisphere. This can be seen in Figures 12a and 12b, which show the HSCT-induced changes for the no PSC and PSC cases, respectively, for 1990 boundary conditions. With the higher levels of background chlorine, the PSC parameterization results in the same general changes as it does with lower chlorine. The increased background chlorine levels slightly increases the sensitivity to to HSCT perturbations in the southern hemisphere high-latitude spring. Elsewhere in the southern hemisphere the response of O_3 to the HSCTs is reduced.

Figures 13a and 13b show the results for the EI = 45 emission scenario. This case differs from the previous emission scenario in that the amount of injected NO_x is 3 times that of the EI = 15 perturbation. Due to the increased NO_x, the maximum depletions in the northern and southern hemispheres exceed 10 DU both with and without the PSCs. The southern hemisphere peak reduction is moved later in the year by the PSCs, as in the EI = 15 case. Again, the global depletion is reduced slightly with the PSCs included in the simulation.

For all the cases studied here, when the PSC parameterization is added the net effect is a reduction in the magnitude of the HSCT O_3 depletion at most latitudes and times of year. At these times and locations, the PSCs act similarly to the sulfate aerosols. The parameterization produces a base model atmosphere that is higher in active chlorine levels and lower in active nitrogen levels than without it. Additional NO_x from the HSCT perturbation is stored in inactive forms, and so not as much O_3 depletion occurs as does without the parameterization.

When the temperature is cold enough, however, PSC surface area densities increase enough from the HSCT perturbation to activate chlorine and increase chlorine-catalyzed loss of O_3. In the southern hemisphere, this is sustained long enough to produce enhanced O_3 depletion compared to the no-PSC case.

At the poles the catalysis of O_3 by the Cl_x cycles involve reactions of ClO with itself and with BrO. The

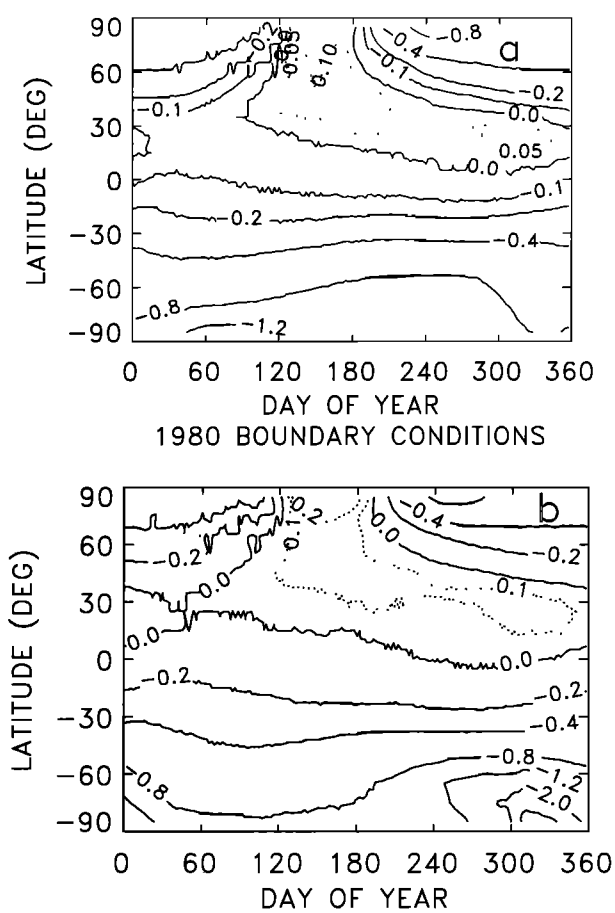

Figure 10. Same as Figure 9, in percent.

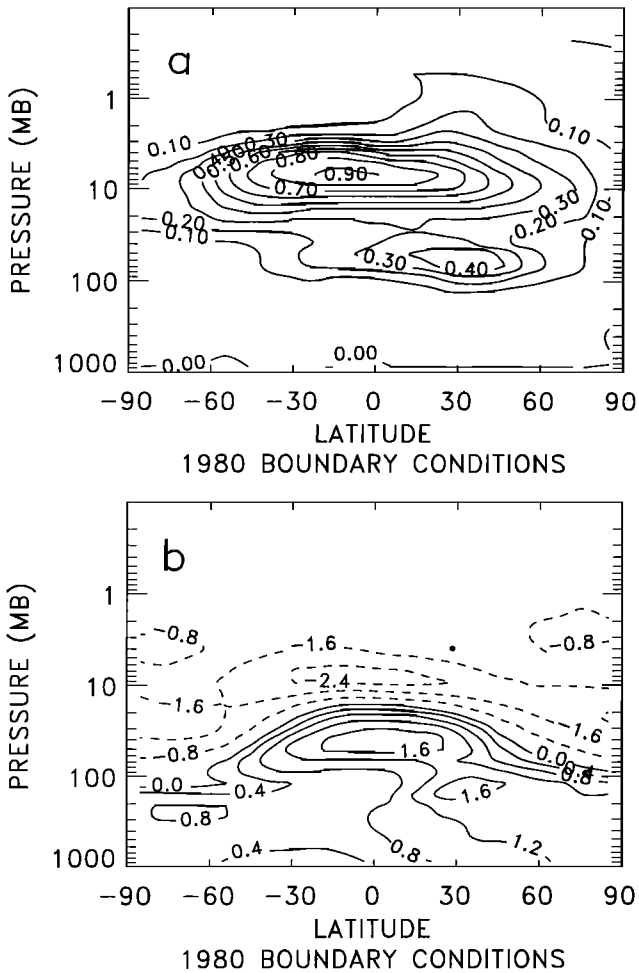

Figure 11. (a) Increase in NO_x in October that results from the EI = 15 HSCT perturbation, in parts per billion by volume. Background chlorine levels approximate 1980 conditions, and no PSC perturbation is included. (b) Percent change in O_3 mixing ratio in October resulting from the EI=15 HSCT perturbation. Dotted lines show decreases in O_3, while solid lines show increases.

ClO dimer cycle is quadratic. In addition, the reaction of ClO with BrO is effectively quadratic, because both increase in response to changes in odd nitrogen partitioning that reduce NO_x and increase HNO_3. In the real atmosphere, the activation of odd chlorine due to the presence of PSCs is expected to be very zonally asymmetric. This raises the question of the validity of the 2-D model formulation, which makes the approximation that $\langle[\mathrm{ClO}]^2\rangle = \langle[\mathrm{ClO}]\rangle^2$ ($\langle\cdot\rangle$ denotes the zonal average). It is easy to see the effects of this approximation by considering a simple longitudinal distribution of ClO, such that

$$\begin{aligned}[\mathrm{ClO}] &= \mathrm{A}, \text{ if } 0 < \lambda \leq \lambda'; \\ [\mathrm{ClO}] &= 0, \text{ if } \lambda' < \lambda \leq 2\pi.\end{aligned} \tag{9}$$

With this distribution, $\langle[\mathrm{ClO}]\rangle^2 = \lambda/2\pi\langle[\mathrm{ClO}]^2\rangle$. The zonal mean approximation underestimates the true rate of O_3 catalysis due to this cycle. Therefore when the HSCT perturbation reduces ClO, the 2-D model will underestimate the resulting decrease in O_3 loss. Similarly, the model will underestimate the increase in O_3 loss that would be caused by an HSCT-induced increase in active ClO. These underestimates would be important at high latitudes because the quadratic catalytic cycles are important there and would depend on the magnitude of the asymmetry in the ClO distribution. It may be possible to use the temperature probability distributions to determine the magnitude of the 2-D model error because high ClO and cold temperatures are highly correlated. This possibility is currently under investigation.

Summary and Conclusion

We have developed a PSC cloud parameterization for use in a 2-D stratospheric model. The key feature of the parameterization is that it uses a statistical description of temperature occurrence to predict the occur-

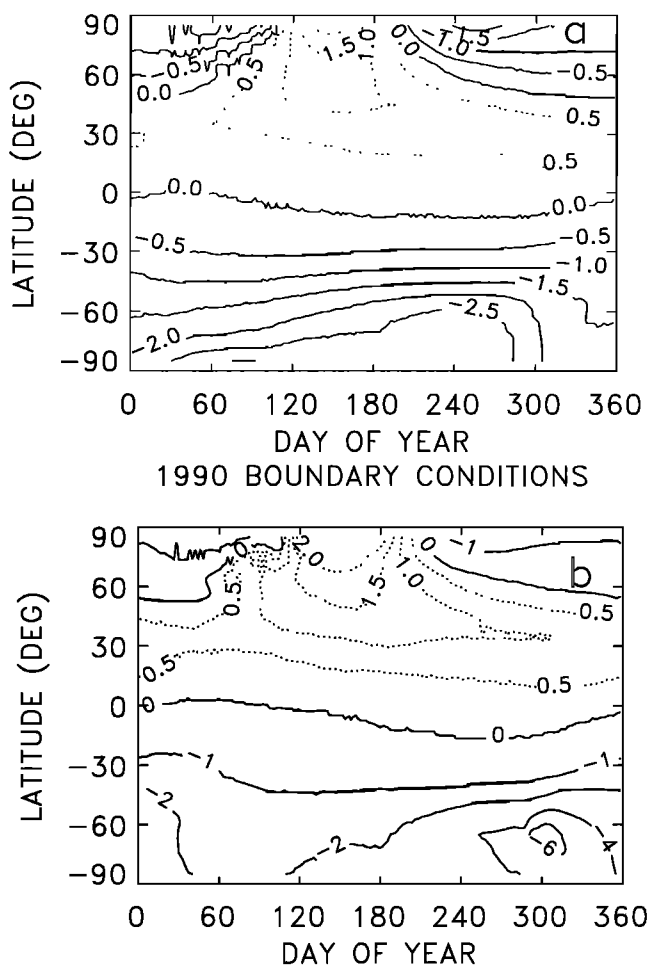

Figure 12. (a) Column O_3 difference resulting from the addition of the EI = 15 HSCT perturbation, in Dobson units, without the PSC parameterization. Background chlorine levels approximate 1990 conditions. Compare with Figure 9a. (b) Column O_3 difference from the HSCTs with the PSC parameterization.

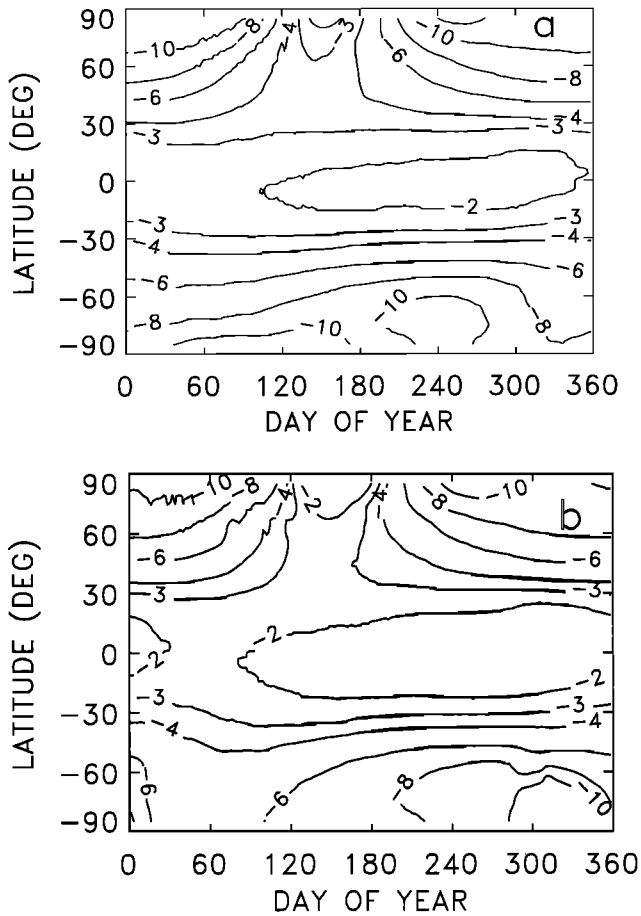

Figure 13. (a) Column O_3 difference resulting from the addition of the EI = 45 HSCT perturbation, in Dobson Units, without the PSC parameterization. Background chlorine levels approximate 1980 conditions. (b) Column O_3 difference from the EI = 45 HSCT case with the PSC parameterization.

rence of PSCs, avoiding the use of zonal mean temperatures. Measurements of NAT and ice aerosol saturation temperatures calculated by *Hanson and Mauersberger* [1988] and *Marti and Mauersberger* [1993], respectively, are combined with supersaturation, sedimentation, and size distribution assumptions to produce PSC occurrence and surface area density climatologies. The parameterization estimates the increase in aerosol formation due to HSCT perturbations. As a result, the effects of PSCs on predictions of HSCT-induced O_3 depletion can be evaluated.

The PSC cloud climatology obtained from the parameterization agrees well with the SAM II observations accumulated over the 1979-1989 period. This demonstrates that the use of a statistical description of stratospheric temperature variations can be used in a 2-D model formulation to predict PSC formation.

The parameterization suggests that PSCs can form in the equatorial regions, in a limited vertical region below 100 mbar. The tropical clouds result in a 1-2% decrease in column O_3. The change in model response to an HSCT perturbation is negligible, however. The incidence of tropical stratospheric clouds may be underestimated in the model due to NO_y values lower than observed. Arbitrarily increasing the NO_y does increase the NAT surface area densities significantly, but the effect on O_3 and model response to HSCT perturbations remains small.

The addition of the PSC parameterization to the model reduces column O_3 and increases active chlorine compared to the model without the parameterization. A feature similar to the ozone hole is generated, with low values of column O_3 occurring in the southern hemisphere late spring/early winter. The low values occur later in the year than is observed in the real atmosphere.

The PSC parameterization improves the agreement with TOMS O_3 trends, with the best agreement in the southern hemisphere. However, it fails to reproduce the large northern midlatitude spring trends observed by the TOMS instrument.

The parameterization has the overall effect of reducing the predictions of column O_3 depletion resulting from an HSCT perturbation. This results because the PSC parameterization increases the importance of the Cl_x catalytic cycle and reduces the importance of the NO_x cycle in the base state. However, in the southern hemisphere spring, the incidence of aerosols and associated heterogeneous processing activates enough Cl_y to significantly increase O_3 depletion compared to a simulation without PSCs.

This behavior has been tested for 1980 and 1990 chlorine levels, and for HSCT emission indices of 15 and 45. It has also been tested with model levels of stratospheric NO_y increased to agree with LIMS observations of lower stratospheric NO_y, with the supersaturation assumptions turned off, and with factor of 4 changes in mean particle radius for both ice and NAT PSCs. (The changes in particle radius also result in large changes in sedimentation rates.) For all these different conditions the basic result remains the same.

The PSC parameterization depends on particle size distribution, supersaturation, and sedimentation assumptions. These are used to avoid the complexity of a microphysical description of PSC behavior but introduce substantial uncertainty into the calculation. However, the results are robust to fairly large changes in these assumptions, and it is likely that they are qualitatively correct.

The use of climatological temperature distributions in 2-D models eliminates the reliance on zonal mean temperatures and allows for a more realistic parameterization to be constructed. This increases the confidence that model predictions made with the improved parameterization correctly capture the behavior of the real stratosphere.

Acknowledgments. The authors would like to thank Mike Pitts at Langley Research Center for providing the SAM II data. Richard Stolarski, Randy Kawa, and Paul Newman and Dave Usinski are also thanked for their helpful comments. The recommendations of two anonymous referees are gratefully acknowledged. This work was partially completed while D. B. Considine held a National Research Council/NASA Resident Research Associateship.

References

Broderick, A. J., A. K. Forney, D. W. Male, and C. J. Scott, Emission characteristics of representative current engines, in Propulsion effluents in the stratosphere: CIAP monograph 2, *U.S. Dep. of Trans., DOT-TST-75-51*, 4.1-4.50, 1975.

Considine, D. B., A. R. Douglass, and R. S. Stolarski, Heterogeneous conversion of N_2O_5 to HNO_3 on background stratospheric aerosols: Comparisons of model results with data, *Geophys. Res. Lett., 19*, 397-400, 1992.

Dopplick, T. G., The heat budget, in *The General Circulation of the Tropical Atmosphere and Interactions with Extratropical Latitudes*, vol. 2, edited by R. E. Newell, J. W. Kidson, D. G. Vincent, and C. J. Boer, pp. 27-94, MIT Press, Cambridge, Mass., 1974.

Dopplick, T. G., Radiative heating of the global atmosphere: Corrigendum, *J. Atmos. Sci., 36*, 1812-1817, 1979.

Douglass, A. R., C. H. Jackman, and R. S. Stolarski, Comparison of model results transporting the odd nitrogen family with results transporting separate odd nitrogen species, *J. Geophys. Res., 94*, 9862-9872, 1989.

Douglass, A. R., C. H. Jackman, R. B. Rood, A. C. Aikin, R. S. Stolarski, M. P. McCormick, and D. W. Fahey, Natural cycles, gases, in The Atmospheric Effects of Stratospheric Aircraft: A First Program Report, *NASA Ref. Publ., 1272*, 33-62, 1992.

Dye, J. E., D. Baumgardner, B. W. Gandrud, S. R. Kawa, K. K. Kelly, M. Loewenstein, G. V. Ferry, K. R. Chan, and B. L. Gary, Particle size distributions in arctic polar stratospheric clouds, growth and freezing of sulfuric acid droplets, and implications for cloud formation, *J. Geophys. Res., 97*, 8015-8034, 1992.

Granier, C., and G. Brasseur, Impact of heterogeneous chemistry on model predictions of ozone changes, *J. Geophys. Res., 97*, 18015-18033, 1992.

Hamill, P., O. B. Toon, and C. S. Kiang, Microphysical processes affecting stratospheric aerosol particles, *J. Atmos. Sci., 34*, 1104-1119, 1977.

Hanson, D., and K. Mauersberger, Laboratory studies of the nitric acid trihydrate: Implications for the south polar stratosphere, *Geophys. Res. Lett., 15*, 855-858, 1988.

Hanson, D., and A. R. Ravishankara, The reaction probabilities of $ClONO_2$ and N_2O_5 on 40 to 75% sulfuric acid solutions, *J. Geophys. Res., 96*, 17307-17314, 1991.

Hofmann, D. J., and S. Solomon, Ozone destruction through heterogeneous chemistry following the eruption of El Chichon, *J. Geophys. Res., 94*, 5029-5041, 1989.

Jackman, C. H., P. D. Guthrie, and J. A. Kaye, An intercomparison of nitrogen-containing species in Nimbus 7 LIMS and SAMS Data, *J. Geophys. Res., 92*, 995-1008, 1987.

Jackman, C. H., R. K. Seals, Jr., and M. J. Prather, Two-dimensional intercomparison of stratospheric models, *NASA CP-3042*, 608 pp., 1989.

Jackman, C. H., A. R. Douglass, R. B. Rood, R. D. McPeters, and P. E. Meade, Effect of solar proton events on the middle atmosphere during the past two solar cycles as computed using a two-dimensional model, *J. Geophys. Res., 95*, 7414-7428, 1990.

Johnston, H., Reduction of stratospheric ozone by nitrogen oxide catalysts from supersonic transport exhaust, *Science, 173*, 517-522, 1971.

Johnston, H., D. E. Kinnison, and D. J. Wuebbles, Nitrogen oxides from high-altitude aircraft: An update of potential effects on ozone, *J. Geophys. Res., 94*, 16351-16363, 1989.

Kasten, F., Falling speed of aerosol particles, *J. Appl. Meteorol., 7*, 944-947, 1968.

Kawa, S. R., D. W. Fahey, K. K. Kelly, J. E. Dye, D. Baumgardner, B. W. Gandrud, M. Loewenstein, G. V. Ferry, and K. R. Chan, The Arctic polar stratospheric cloud aerosol: Aircraft measurements of reactive nitrogen, total water, and particles, *J. Geophys. Res., 97*, 7925-7938, 1992.

Ko, M. K. W., M. B. McElroy, D. K. Weisenstein, and N. D. Sze, Lightning: A possible source of stratospheric odd nitrogen, *J. Geophys. Res., 91*, 5539-5404, 1986.

Ko, M. K. W., Ozone response to aircraft emissions: Sensitivity studies with two-dimensional models, in The Atmospheric Effects of Stratospheric Aircraft: A First Program Report, *NASA Ref. Publ.*, 1272, 115-157, 1992.

Ko, M. K. W., and D. Weisenstein, Ozone response to aircraft emissions: Sensitivity to heterogeneous reactions, in The Atmospheric Effects of Stratospheric Aircraft: A Second Program Report, *NASA Ref. Publ.*, 1293, 83-113, 1993.

Ko, M. K. W., and A. R. Douglass, Update of model simulations for the effects of stratospheric aircraft, in The Atmospheric Effects of Stratospheric Aircraft: A Third Program Report, *NASA Ref. Publ.*, 13133, 209-244, 1993.

McCormick, M. P., and C. R. Trepte, SAM II measurements of Antarctic PSCs and aerosols, *Geophys. Res. Lett., 13*, 1276-1279, 1986.

Marti, J. and K. Mauersberger, A survey and new measurements of ice vapor pressure at temperatures between 170 and 250 K, *Geophys. Res. Lett., 20*, 363-366, 1993.

Miake-Lye, R. C., Designing a methodology for future air travel scenarios, in The Atmospheric Effects of Stratospheric Aircraft: A First Program Report, *NASA Ref. Publ.*, 1272, 13-32, 1992.

Peter, T., C. Bruhl, and P. J. Crutzen, Increase in the PSC-formation probability caused by high-flying aircraft, *Geophys. Res. Lett., 18*, 1465-1468, 1991.

Pitts, M. C., L. R. Poole, and M. P. McCormick, Polar stratospheric cloud sightings by SAM II, 1979-1989: Contrasts between the Antarctic and Arctic, *Eos Trans. AGU, 72*, 77, 1991.

Poole, L. R., S. Solomon, B. W. Gandrud, K. A. Powell, J. E. Dye, R. L. Jones, and D. S. McKenna, The polar stratospheric cloud of January 24, 1989, 1, Microphysics, *Geophys. Res. Lett., 17*, 537-540, 1990.

Rosenfield, J. E., M. R. Schoeberl, and M. A. Geller, A computation of the stratospheric diabatic residual circulation using an accurate radiative transfer model, *J. Atmos. Sci., 44*, 859-876, 1987.

Solomon, S., Progress towards a quantitative understanding of Antarctic ozone depletion, *Nature, 347*, 347-354, 1990.

Stolarski, R. S., P. Bloomfield, R. D. McPeters, and J. R. Herman, Total ozone trends deduced from Nimbus 7 TOMS data, *Geophys. Res. Lett., 18*, 1015-1018, 1991.

Turco, R. P., R. C. Whitten, and O.B. Toon, Stratospheric aerosols: Observation and theory, *Rev. Geophys., 20*, 233-279, 1982.

Turco, R. P., O. B. Toon, and P. Hamill Heterogeneous physicochemistry of the polar ozone hole, *J. Geophys. Res., 94*, 16493-16510, 1989.

Weisenstein, D., M. K. W. Ko, J. M. Rodriguez, and N. D. Sze, Impact of heterogeneous chemistry on model-calculated ozone change due to HSCT aircraft, *Geophys. Res. Lett., 18*, 1991-1994, 1991.

Wofsy, S. C., G. P. Gobbi, R. J. Salawitch, and M. B. McElroy, Nucleation and growth of $HNO_3 \cdot H_2O$ particles in the polar stratosphere, *J. Atmos. Sci., 47*, 2004-2012, 1990.

World Meteorological Organization (WMO), Scientific assessment of stratospheric ozone: 1989, Global Ozone Res.

and Monit. Proj., World Meteorol. Org., *Rep. 20*, Geneva, 1990.

World Meteorological Organization (WMO), Scientific assessment of stratospheric ozone: 1991, Global Ozone Res. and Monit. Proj., World Meteorol. Org., *Rep. 25*, Geneva, 1992.

D. B. Considine, A. R. Douglass, and C. H. Jackman, Code 916, NASA Goddard Space Flight Center, Greenbelt, MD 20771.

(Received June 29, 1993; revised February 4, 1994; accepted April 14, 1994.)